Structure of ATP-Bound Human ATP:Cobalamin Adenosyltransferase†

Heidi L. Schubert* and Christopher P. Hill

Department of Biochemistry, University of Utah, Salt Lake City, Utah 84112-5650

Received July 11, 2006; Revised Manuscript Received October 20, 2006

ABSTRACT: Mutations in the gene encoding human ATP:cobalamin adenosyltransferase (hATR) can result in the metabolic disorder known as methylmalonic aciduria (MMA). This enzyme catalyzes the final step in the conversion of cyanocobalamin (vitamin B_{12}) to the essential human cofactor adenosylcobalamin. Here we present the 2.5 Å crystal structure of ATP bound to hATR refined to an R_{free} value of 25.2%. The enzyme forms a tightly associated trimer, where the monomer comprises a five-helix bundle and the active sites lie on the subunit interfaces. Only two of the three active sites within the trimer contain the bound ATP substrate, thereby providing examples of apo- and substrate-bound-active sites within the same crystal structure. Comparison of the empty and occupied sites indicates that twenty residues at the enzyme's N-terminus become ordered upon binding of ATP to form a novel ATP-binding site and an extended cleft that likely binds cobalamin. The structure explains the role of 20 invariant residues; six are involved in ATP binding, including Arg190, which hydrogen bonds to ATP atoms on both sides of the scissile bond. Ten of the hydrogen bonds are required for structural stability, and four are in positions to interact with cobalamin. The structure also reveals how the point mutations that cause MMA are deficient in these functions.

Cobalamin functions as an enzymatic cofactor for a variety of metabolic reactions, including methionine synthesis, succinyl-CoA synthesis, and fermentation of small molecules (*1*−*3*). In mammalian systems, vitamin B_{12} (cyanocobalamin, CNCbl)[1] is ingested and converted into two cofactors, methylcobalamin (MeCbl) and adenosylcobalamin (AdoCbl), each of which is required for an essential catalytic activity. MeCbl is the cofactor for methionine synthase, which converts homocysteine to methionine (*4*, *5*). Adenosylcobalamin (AdoCbl) is the cofactor for methylmalonyl CoA mutase (MMCM), which catalyzes the isomerization of methylmalonyl CoA to succinyl CoA and is responsible for normal catabolism of various amino and fatty acids through the tricarboxylic acid (TCA) cycle (*6*).

The conversion from CNCbl to the active cofactors requires carrier proteins, membrane transport, cobalt reduction, and exchange of the axial ligand (*7*−*10*). Genetic alterations in the branched modification pathway can disrupt either MeCbl or AdoCbl production or both (*11*, *12*). The disruptions at particular points in the pathway can be physiologically distinguished based on enzymatic activities, blood plasma analysis, and medical responsiveness to various cobalamin analogue treatments (*13*). These inborn errors in vitamin B_{12} metabolism have been categorized into eight complementation classes, *cblABCDEFG* and *mut* (*14*, *15*). Loss of AdoCbl results in methylmalonic aciduria (MMA), a buildup of methylmalonic acid in body fluids, including blood and urine (*12*, *16*). Mutations in three different genetic loci, *cblA*, *cblB*, and *mut*, specifically result in AdoCbl deficiency. Methylmalonyl CoA-mutase is encoded at the *mut* locus (*17*), *cblA* was mapped to an uncharacterized enzyme with GTPase activity (*18*), and the deficient enzyme of the *cblB* class was identified as ATP:cobalamin adenosyltransferase (ATR) (*19*). A BLAST search of the human genome using an *Archaeoglobus fulgidus* ATR homologue, review of mutations in the genes of MMA patients, and bacterial complementation studies subsequently revealed the gene encoding the human ATR homolog (hATR), named hMMAB (*20*, *21*). Sequencing of hMMAB in MMA patients revealed 32 different types of mutations, including six point mutations. MMA patient cell lines containing hATR mutations show reduced AdoCbl levels *in vitro* (*20*, *22*, *23*).

ATP:Cobalamin adenosyltransferase catalyzes transfer of adenosine from ATP to cobalamin to generate AdoCbl. The PduO-family of adenosyltransfreases has a strong preference for ATP, and other nucleotides are inefficient donors to cobalamin (*24*−*26*). Prior to catalytically relevant binding, cob(III)alamin is reduced to cob(II)alamin by single electron reduction, a reaction catalyzed by a reductase such as flavodoxin or methionine synthase reductase (*26*, *27*). If the hATR is preincubated with ATP, the binding of cob(II)alamin triggers a transition to a novel four-coordinate cob(II)alamin (*28*, *29*). This is followed by a second single electron reduction at the cobalt center to produce enzyme-bound cob(I)alamin, a step that might be catalyzed by methionine

* To whom correspondence should be addressed. Telephone: 801-585-3919. Fax: 801-581-7959. E-mail: heidi@biochem.utah.edu.

† This work was supported by the NIH grant GM56775. Data collection at NSLS was supported by the Offices of Biological and Environmental Research and of Basic Energy Sciences of the U.S. Department of Energy/National Center for Research Resources of the NIH.

[1] Abbreviations: ATP, adenosine triphosphate; Cbl, cobalamin; CNCbl, cyanocobalamin; MeCbl, methylcobalamin; AdoCbl, adenosylcobalamin; OHCbl, hydroxycobalamin; MMCA, methylmalonyl CoA Mutase; MMA, methylmalonic aciduria; MMAB, MMA gene for complementation group CblB; ATR, adeonsyltransferase; rms, root mean square; EPR, electron paramagnetic resonance; MCD, magnetic circular dichroism.

10.1021/bi061396f CCC: $33.50
Published on Web 12/06/2006 PAGE EST: 8

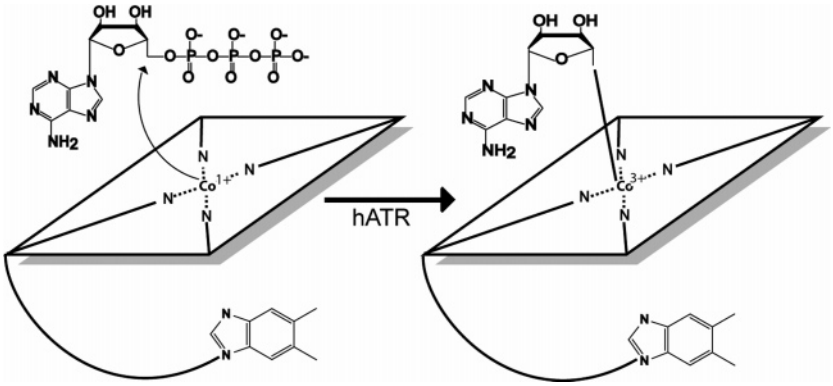

FIGURE 1: Schematic outline of the reaction catalyzed by ATP:cobalamin adenosyltransferase.

synthase reductase (*26*). Interactions between the ATR and the cob(II)alamin are thought to lower the reduction potential of the cobalt into the physiologically accessible range (*30*, *31*). Finally, while bound to hATR, the four-coordinate cob(I)alamin attacks the C5* atom of the bound ATP to release the triphosphate group and form the cobalt−carbon bond of adenosylcobalamin (Figure 1). The roles of specific hATR residues in the course of this reaction are unknown.

Sequence analysis indicates that ATP:cobalamin adenosyltransferases fall within three unrelated families: CobA, PduO, and EutT (*24*). Structure determinations confirm that the CobA (*32*) and PduO (*25*) families adopt quite different architectures; a structure has not yet been described for a member of the EutT family. Human ATR belongs to the PduO-like family, which, as indicated by the structure of archaeal *Thermoplasma acidophilium* TA0546, adopts a helical bundle fold that assembles as a stable trimer (*25*). This structure (32% identical to hATR) was determined in the apo state, as were six other sequence-related proteins that are thought to have ATR activity. Because these structures lack bound ligands, the detailed location of the active site and the function of specific invariant residues are unknown.

In an effort to better understand the PduO-like ATR family, and the human enzyme in particular, we have determined the structure of hATR in the presence of ATP. This structure reveals previously unstructured invariant residues at the N-terminus, the functional role of the invariant residues surrounding the ATP, the putative location of the cobalamin-binding site, and residues likely to be involved in the catalytic mechanism.

METHODS

A human MMAB clone, starting at the equivalent region of the sequence as previously crystallized homologues (Pro56), was generated from I.M.A.G.E. clone 2822202 (ATCC) and inserted into a pET3a vector (Invitrogen). Sequencing determined that the clone is the Lys239 variant (*20*). No affinity tag is present, but an initiator Met was added using the Nde1 restriction enzyme during cloning. The recombinant hATR was overexpressed in *E. coli* using an auto-induction method (*33*). Cell pellets were lysed by sonication in 20 mM HEPES, pH 7.5, 50 mM NaCl, 1 mM DTT and centrifuged to remove the particulate fraction. The soluble lysate was loaded onto a HiTrap SP HP column (Pharmacia) and eluted by a salt gradient at 300 mM NaCl. The protein was relatively pure at this stage but was dialyzed against 20 mM HEPES, pH 7.5, 100 mM NaCl, 1 mM DTT, concentrated, and further purified by size exclusion chromatography on an SD100 column (Pharmacia). The protein was concentrated to 20 mg ml^{-1} for crystallization trials in the presence of 1−5 mM MgATP. Lower or higher ATP concentrations did not yield crystals.

Table 1: Data Collection

crystal data	
space group	*P*321
no. observations	113031
no. unique reflections	29063
resolution range (Å)	50 − 2.5
(high resolution shell)	(2.59 − 2.5)
completeness (%)	99.8 (100)
$I/\sigma(I)$	9 (2)
R_{sym}[a] (%)	13.6 (56)
Wilson B (Å^2)[b]	46.2
R_{cryst}[c] (%)	19.9 (22)
R_{free}[c] (%)	25.2 (25)
rms deviations	
bonds (Å)	0.013
angles (deg)	1.5
$\langle B \rangle$ (Å^2)	
main chain	33.7
side chain	34.9
ATP (2)	25.8
SO_4 (3)	60.4
Mg (4)	35.8
Cl (1)	33.4
H_2O (171)	32.7

[a] $R_{sym} = 100 \times \Sigma|I - \langle I \rangle|/\Sigma I$, where $\langle I \rangle$ is the average intensity from multiple observations of symmetry related reflections. [b] The Wilson B was calculated using TRUNCATE between 4 and 2.5 Å resolution and contains an error of ± 10 Å^2 (*36*). [c] $R_{cryst} = 100 \times \Sigma||F_o| - |F_c||/\Sigma|F_o|$ over 95% of the data. $R_{free} = R_{cryst}$ on 5% of the data not used in refinement.

hATR−ATP crystals were grown by vapor diffusion at room temperature by mixing 2 μL of protein solution with 2 μL of reservoir (18−20% polyethyleneglycol, MW = 3350, 0.2 M $MgSO_4$ and 10% glycerol). The crystals belong to space group *P*321, with cell dimensions of $a = b = 111.2$ Å, $c = 115.5$ Å, and have three molecules in the asymmetric unit. Native data were collected at the National Synchrotron Light Source (Brookhaven, NY) beamline x26c (Table 1). The structure was determined by molecular replacement (PHASER (*34*)) using a model of hATR based on the trimeric structure of the *Bacillus subtilus* YVQK (41% identical to hATR; 1RTY). Residues of helical regions were modeled as the equivalent human sequence and flexible loops were removed prior to molecular replacement. The primary

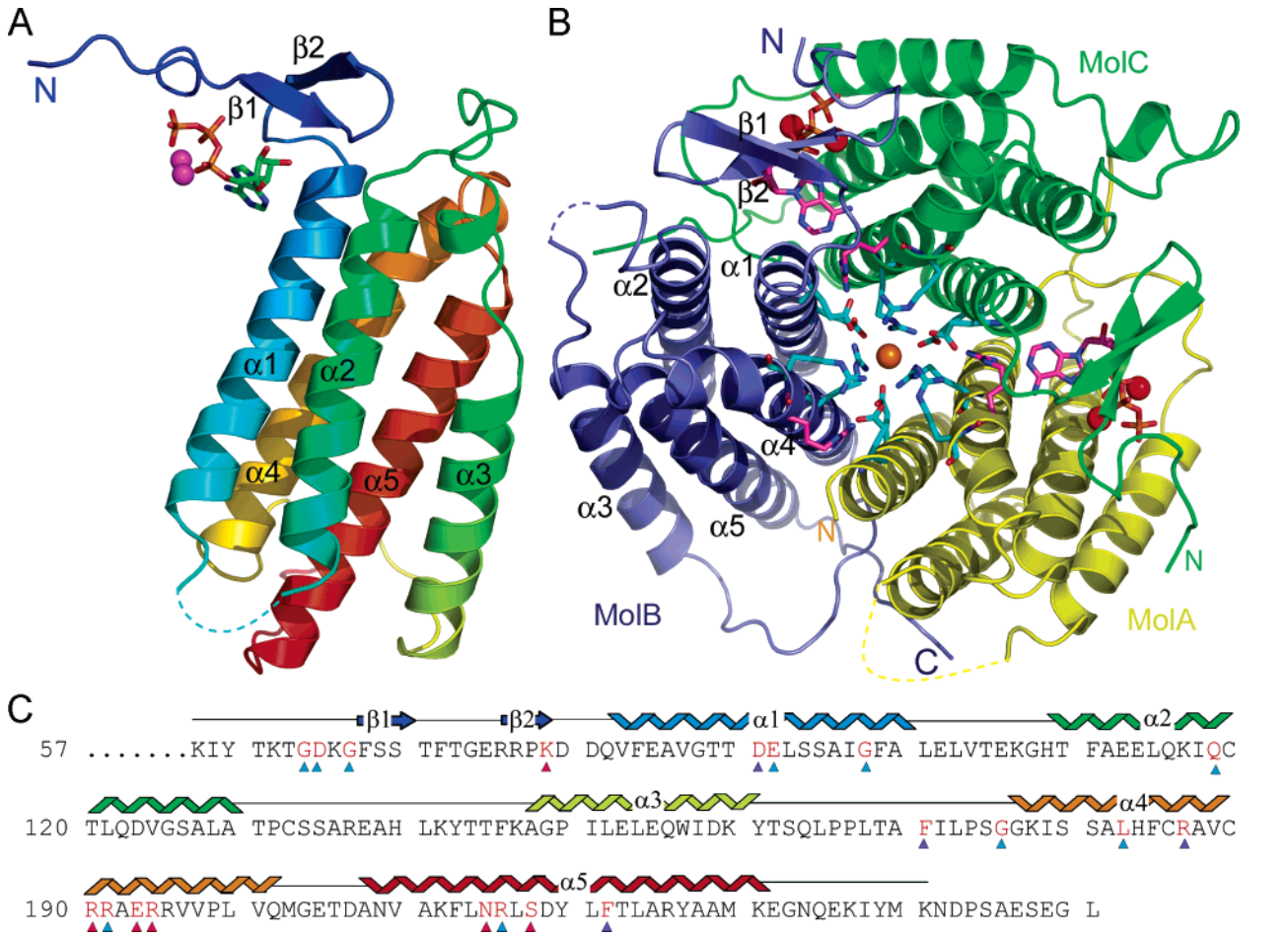

FIGURE 2: Structure of hATR. (A) Side view of the hATR monomer. The trace is colored blue from the N-terminus to red at the C-terminus. The N-terminal portion is only ordered in the presence of bound ATP; molecule C is shown. (B) Top view of the hATR trimer. Molecules A, B, and C are colored yellow, blue, and green, respectively. ATP molecules (magenta) with two Mg^{2+} ions each (red) are bound at the AC and CB interfaces underneath the ordered N-terminal β-strands. The apo-active site sits at the BA interface. The trimer interface formed by the supercoil of helices α1 and α4 contains alternating Glu/Arg residues (Glu84/Arg195 and Glu91/Arg191 (cyan)). This charged network connects via Glu84 to the ATP-binding site though a hydrogen bond to invariant Arg194 (magenta). A chloride ion has been modeled in the center of the charged ring (orange). Two rings of phenylalanine side chains lie on the trimer interface below the Arg/Glu pairs and are omitted from this figure for clarity. (C) Sequence of the hATR with invariant resides highlighted in red, as determined by the extended sequence alignment included in the Supporting Information. Secondary structure is shown above and colored as in Figure 2a. Colored triangles below the sequence denote the functional role of the invariant residues (Table 2) (ATP binding, red; cobalamin binding pocket, blue; structural function, cyan). Figures 2a,b and 3, 4, and 5 were made with PYMOL (*45*).

programs used for structure determination and model building were HKL (*35*), CCP4 (*36*), O (*37*), and Coot (*38*).

The hATR construct, residues 56−250 (C-terminus), includes all of the highly conserved amino acids (Supporting Information). The missing upstream region includes the predicted mitochondrial targeting sequence, residues 1−32. The following ordered residues are included in the refined model: A79−129, A144−240, B57−135, B142−240, C58−104, and C108−240. Two of the trimer's active sites are seen to each bind one ATP molecule and two Mg^{2+} ions. The final model has been refined at a resolution of 2.5 Å using REFMAC (*39*) to an *R* factor of 19.8% with an R_{free} value of 25.2% and good geometry (Table 1). The structural coordinates have been deposited at the RCSB Protein Data Bank (PDB) with deposition code 2IDX.

Related cobalamin adenosyltransferase structures were identified by using the program DALI (*40*), the Protein Structure Comparison Service (*41*), and by running a BLAST search using the PDB as the amino acid sequence database. A survey of ATP-binding sites was completed by visually scanning all non-redundant PDB entries that contained ATP as a ligand (~266 structures).

RESULTS AND DISCUSSION

Structure of the hATR Monomer. The hATR monomer adopts a helical ferritin-like architecture (Figure 2) (*42*). Structures of this type are defined by their organization of four helices; α1, α2, α4, and α5 of hATR. These four helices form a bundle in which spatially adjacent helices are antiparallel to each other. The PduO-type cobalamin adenosyltransferase family is distinguished by an additional helix, α3 of hATR, which is located in the long loop that connects α2 to α4 (Figure 2a). Although ferritin contains a similar four-helical bundle arrangement, its long-crossover loop does not contain a helix and it wraps around the bundle in the opposite sense to that of the PduO-type cobalamin adenosyltransferases.

ATR activity has been confirmed, and the structure has been described for the *Thermoplasma acidophilum* protein 0546 (1NOG), which is 32% identical to hATR (*25*). Several

Table 2: Invariant Residues and Their Function within the hATR Structure[a]

invariant residue	function
Gly63	forms a tight turn to allow close proximity of β-strands to active site
Asp64	forms salt bridge with Arg215 to hold N-terminal loop in place
Gly66	within a tight turn of the N-terminal loop
Lys78	H-bonds directly with a β-phosphate, Glu193, water, and N-terminal loop
Asp90	potential interaction with cobalamin
Glu91	salt bridge with Arg191 at center of trimeric interface
Gly97*	positioned on α1 and allows close approach of the α3−α4 loop
Gln118	sits on α2 and H-bonds the α3−α4 loop and back to α1
Phe170	potential interaction with cobalamin
Gly175	finishes the α3−α4 loop and starts α4
Leu182	hydrophobic core
Arg186*	potential interaction with cobalamin
Arg190*	H-bonds with all three sections of ATP and on either side of scissile bond
Arg191*	salt bridge with Glu91 at center of trimer interface
Glu193*	H-bonds with one Mg−HOH and NZ of Lys78
Arg194	forms H-bond with adenosine N1 and leads to charged trimeric interface through H-bond to Glu84; also forms water mediated H-bond to Asp90
Asn214	a direct ligand to Mg^{2+} and two γ-phosphate oxygens
Arg215	salt bridge with Asp64 locking down N-terminal loop and ATP-binding cleft
Ser217	forms H-bond to Mg−HOH
Phe221	potential interaction with cobalamin

[a] Residues marked with an asterix have been identified as point mutations in MMA patients (*20*, *22*, *23*).

other related structures of probable ATR enzymes have also been reported by proteomics consortia, including *Bacillus subtilis* YVQK (1RTY), *Sulfolobus tokodaii* ST2180 (1WVT), *Sulfolobus Tokodaii* ST1454 (1WOZ), *Bacillus halodurans* 10174212 (2AH6), *Mycobacterium tuberculosis* Mb1347c (2G2D), and *Pyrococcus horikoshi* OT3 PH0671 (1WY1). A sequence alignment containing a range of species and all known crystal structures is presented in the Supporting Information. The list of invariant residues as defined by this alignment is shown in Figure 2c and listed in Table 2. Of these structures, the most similar sequence (41% identical) to the human enzyme is for *Bacillus subtilis* YVQK, which was used for the molecular replacement solution. The rms deviation between these related structures and hATR is typically 1.2−2.0 Å over ∼140 Cα residues. Interestingly, *Thermoplasma acidiphilum* TA1238 (1NIG) contains a short fifth helix indicative of the cobalamin ATR family but does not contain the conserved amino acids that are thought to function in ATP or cobalamin binding (*43*). None of these structures were determined in the presence of ATP, leaving the structure and functional role of many conserved resides unknown.

Structure of the hATR Trimer. Human ATR is a trimer in the crystal and in solution, as indicated by gel filtration chromatography. Helices α1 and α4 of each monomer associate to form the six-stranded coiled-coil core of the trimer (Figure 2b). All of the related structures listed above also crystallize in the same trimeric arrangement, with the *T. acidophilum* 0546 and *Mycobacterium tuberculosis* Mb1347c enzymes trimerizing about a crystallographic 3-fold axis and the others associating via noncrystallographic symmetry. Toward the top of the structure (closer to the ATP-binding site; Figure 2b), the trimer interface contains two charged rings of Arg/Glu pairs (Glu84/Arg195 and Glu91/Arg191) that surround what appears to be a chloride ion. Glu84 from the topmost ring also forms a hydrogen bond with the guanidinium of the invariant Arg194 residue, which in turn hydrogen bonds to the N1 nitrogen of the bound ATP, thereby connecting the trimer interface to the active site. Below these two rings of charged residues lie two additional rings of phenylalanines (conserved as hydrophobic residues) that form a solid core to the interface. The hATR subunit interfaces are extensive (the apo- and substrate-bound interfaces cover 895 and 1450 $Å^2$) and are mediated by conserved residues, thereby indicating that the formation of the trimer is required for activity.

Although the presence of differently occupied active sites could indicate allostery within the trimer, we do not favor this possibility because superposition of occupied and unoccupied subunits does not reveal an obvious pathway of conformational changes that might mediate communication between the active sites. The rms deviation between the three subunits using pairs of equivalent Cα atoms is only 0.73−0.78 Å (Figure 3c), although as discussed below, there are some distinctive differences at the active sites. It seems more likely that crystal contacts at each active site stabilize or prohibit conformations that are able to bind ATP. Curiously, cobalamin is also seen bound to just one of the two active sites in the crystal structure of dimeric CobA, which is structurally unrelated to ATR but catalyzes the same reaction (*32*). Biochemical studies indicated that, as appears be the case for hATR, the structural asymmetry of CobA is a crystallographic artifact and is probably not of mechanistic significance (*44*).

ATP-Binding Site. The location of the ATP-binding site at the interface between adjacent monomers further indicates that ATR is functional as a trimer. Notably, the three active sites in the asymmetric unit are distinctly different, with only two of them containing ATP and the other (between molecules A and B) being unliganded (Figures 2b and 3). The active site cleft is formed between the α1 and α2 of one monomer and the α3−α4 loop and α4 and α5 of its neighbor and is lined by many conserved residues. Comparison of bound- and apo-active sites reveals that binding of ATP triggers a significant local ordering of the structure. N-terminal residues surrounding the apo-active site are disordered before residue 79 (Figure 3a,d), whereas active sites occupied by ATP are ordered from residue 57 or 58 (2 or 3 residues after the N-terminus of this construct) (Figure 3b,e,f). The cleft formed by the ordered N-terminus is a deep

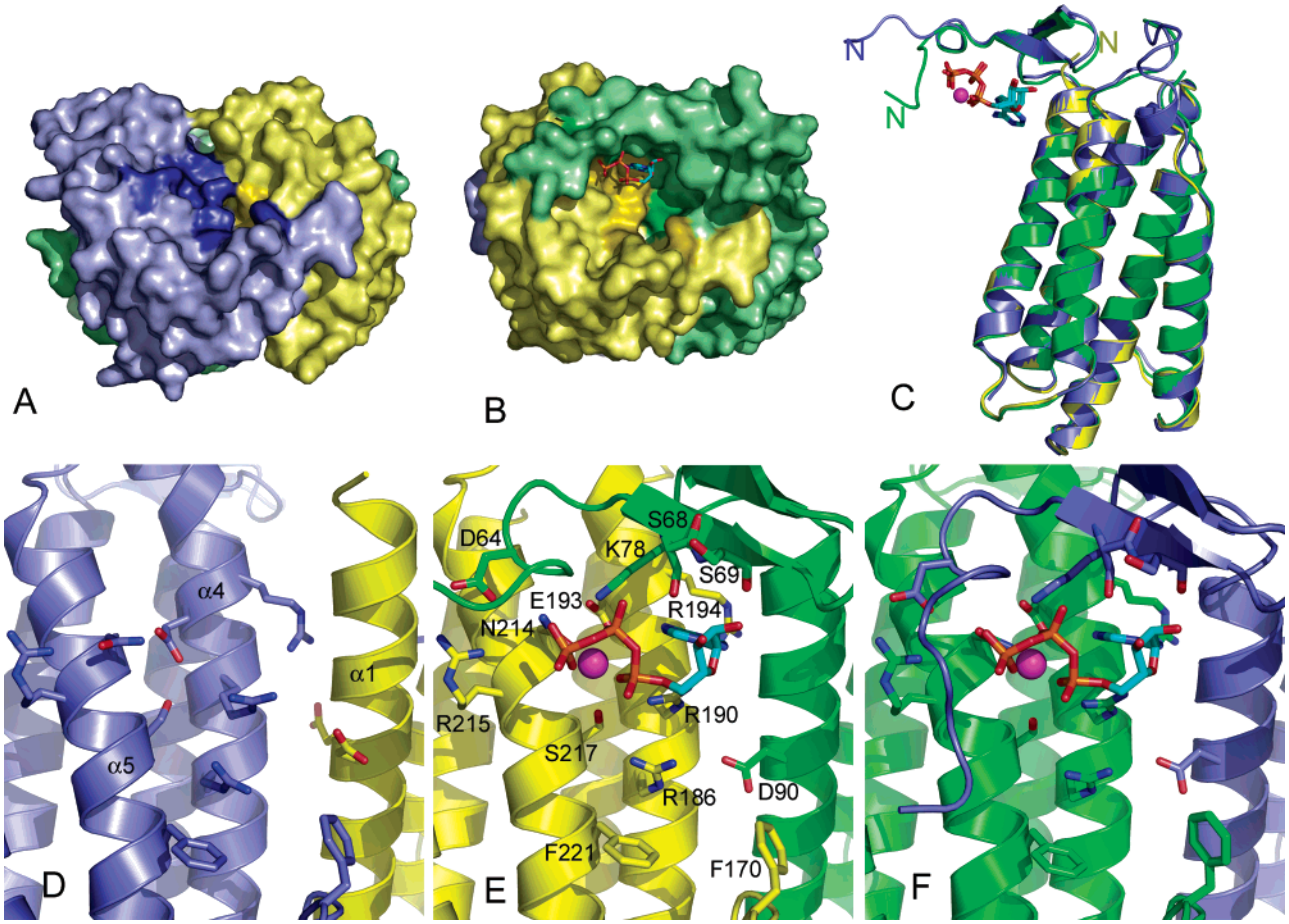

FIGURE 3: Side view of the hATR active sites. (A) Surface of the apo-active site (at the BA interface) reveals several exposed invariant residues. The figure is colored as in Figure 2b with invariant residues in darker hue. The right-hand molecule, molecule A (yellow), is only ordered from residue 79. (B) An ATP-bound-active site (the AC active site is shown in the same orientation as in panel A) reveals the ordered N-terminal residues of the right-hand molecule, molecule C (green), starting at residue 57, and wrapping over the top of the bound ATP (ball-and-stick). (C) All three monomers are aligned, revealing close structural similarity except at the N-terminus where binding of ATP causes ordering of ~22 N-terminal residues in molecules B and C. (D) Detailed view of the apo-active site (the BA interface). (E) ATP-bound-active site at the AC interface with residues involved in binding ATP or positioned in the putative cobalamin binding pocket (Arg186, Phe170, Phe221, Asp90). All labeled residues are invariant except Ser68 and Ser69. (F) ATP-bound-active site of the BC interface reveals slight differences in the extreme N-terminus of molecules B and C.

pocket slightly bigger than twice the size of the bound ATP. This conformational change suggests that binding of ATP contributes to formation of the cobalamin binding site. The structurally unrelated CobA-type ATP:cobalamin adenosyltransferase has also been shown to increase in structural order with the binding of substrates (*32*).

Nucleotide binding to hATR involves the formation of numerous hydrogen bonds and van der Waals contacts. ATP binds with the adenosine ring inserting toward the core of the enzyme and the ribose hydroxyls and several phosphate oxygens in solvent accessible positions (Figure 4a,b). The adenosine lies near strands β1, β2, and helix α1, which is a region previously proposed to be involved in nucleotide binding (*21*). A search of ATR-like structures and of ATP-bound protein structures did not reveal a similar mode of nucleotide binding, indicating that hATR contains a novel type of ATP-binding site. Hydrogen bonds extend from the adenosine amide group (N6) to both the side chain of Glu193 and the main-chain carboxyl of Arg190 (Figure 4b, Table 2). The adenosine N1 nitrogen hydrogen bonds with the side chain of Arg194, and this interaction connects the ATP-binding pocket to the topmost charged ring of the trimer interface through a second hydrogen bond between Arg194 and Glu84. Finally, the adenosine N3 nitrogen packs against the conserved residue Gly87 and explains why PduO-like ATRs prefer ATP as the nucleotide donor over GTP. Although hATR is 16% efficient at using GTP as the nucleotide donor (*26*), activity with GTP is below measurable levels for the *T. acidophilum* TA1434 and *Salmonella* PduO enzymes (*24*, *25*). In contrast, CobA-like ATRs have fewer hydrogen bonds between the adenosine and the enzyme, consistent with their nucleotide promiscuity (*32*).

The Arg190 guanidinium group packs against the five-membered ring of the nucleotide and also hydrogen bonds with the ribose oxygen. The ring oxygen (O4*) and the phosphate bridging oxygen (O5*), which are on opposite sides of the scissile C5*−O5* bond, both interact with the side chain of Arg190 (Figure 4). An additional hydrogen bond is formed between the ribose O2* hydroxyl and the main-chain carbonyl oxygen of Ser69. Finally, hydrophobic contacts between Phe83 and the ribose ring, and between nearby Gly87 and a portion of the adenosine ring, further define the ATP-binding conformation. Together, these contacts work to orient the C5* atom toward the putative cobalamin binding site (Figure 4).

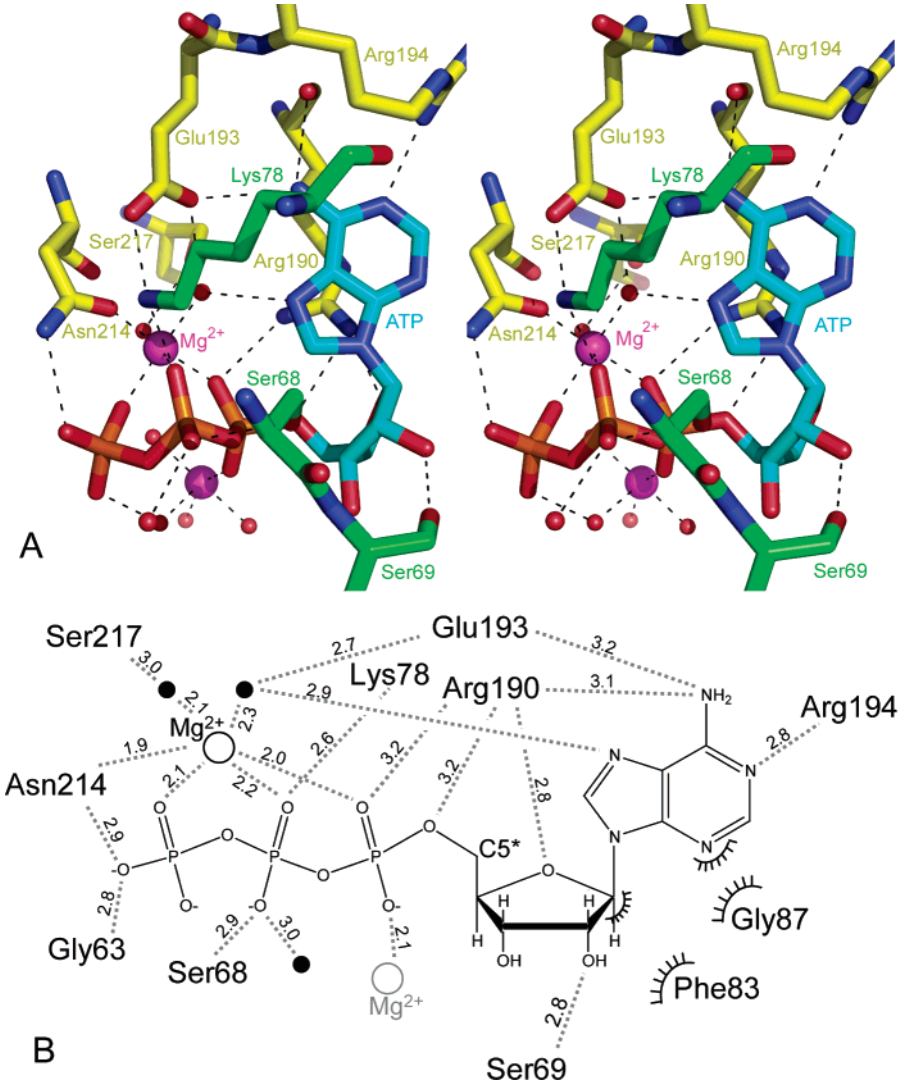

FIGURE 4: ATP-binding site. (A) The ATP-binding site is shown in stereo. Invariant residues that are involved in forming hydrogen bonds to the bound ATP are shown explicitly. The hydrogen bond from nonconserved Ser69 extends from its main-chain carbonyl not its hydroxyl side chain. Two Mg^{2+} ions interact with the triphosphate moiety. Arg194 recognizes the adenosine and connects this interaction to the trimer core. (B) Schematic representation of ATP-binding site and interactions with hATR residues. Hydrogen bonds are shown as dashed lines with distances shown in angstroms. Waters and Mg^{2+} are shown as closed and open circles. The secondary Mg, which is likely not physiologically relevant, is shown in gray. Ser68, Phe83, and Gly87 are conserved but not invariant.

The three phosphates pack against the N-terminal loop of one subunit and helices α4 and α5 of the adjacent subunit (Figures 3e,f and 4a). Two Mg^{2+} ions have been modeled coordinating the phosphates, one of which binds oxygen atoms from all three phosphate groups, two water molecules, and the side-chain oxygen atom of invariant Asn214. Because Asn214 also hydrogen bonds with Asp64, this interaction may be especially important for ordering of the N-terminal residues upon binding of ATP (Figure 3e,f). The other modeled Mg^{2+} ion is located in a much more solvent accessible environment and may be the result of high concentrations of $MgSO_4$ in the crystallization conditions rather than indicating a physiologically significant coordination. Phosphate oxygens also form hydrogen bonds with the side chains of the invariant residues Asn214 and Arg190, the carbonyl of Gly63, and with the hydroxyl Ser68 (conserved Ser/Thr; Supporting Information, Figure 4a,b).

Cobalamin Binding Site. The ordering of hATR N-terminal residues that occurs upon binding of ATP induces formation of an active site cleft that not only holds ATP but also contains an oval-shaped opening that measures 14 × 8 Å and is 7 Å deep (Figure 3b). The top of this presumed cobalamin binding cleft is bounded by the ATP molecule itself, and the ATP C5* atom is oriented toward the center of the pocket as if poised for catalysis. The surface of the cleft includes four invariant residues (Asp90, Phe170, Arg186, and Phe221) that are not involved in binding ATP but could potentially interact with cobalamin (Figure 3e,f). The invariant side chain of Arg186 projects just below the ATP and is a candidate for binding the cobalamin directly, perhaps to the side-chain amides. Asp90 appears well placed to interact with the bound cobalamin or may function in catalysis. Two invariant phenylalanine residues, Phe170 and Phe221, project into the active site cleft and are good candidates for binding the hydrophobic surfaces of cobalamin or the dimethylbenzimidazole (DMB) tail.

Modeling Cobalamin Binding. A key question to understanding the mechanism of hATR is the conformation of cobalamin when bound to the enzyme, because this can dramatically alter reactivity at the Co center. UV−vis, EPR,

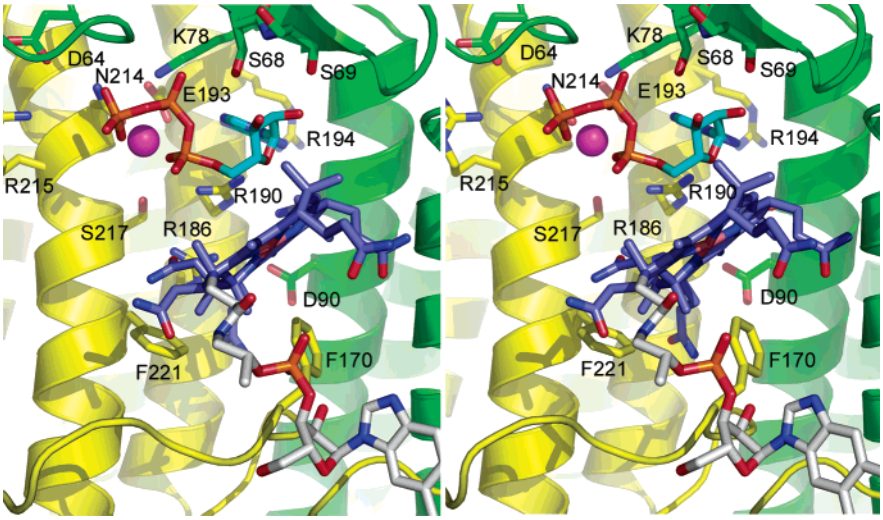

FIGURE 5: Model of base-off cobalamin bound to the active site, shown in stereo in the same orientation as Figure 3e. The model is not intended to imply specific residue interactions, but rather to provide a sense of scale and demonstrate the plausibility of the apparent cobalamin binding pocket. The corrin ring (blue) is positioned ~4 Å away from the ATP (cyan), and the amide side chains of the A- and B-rings point toward the base of the binding cleft. The benzimidazole tail (white) is extended away from the structure in a position that is highly speculative in the absence of additional structural information.

and MCD spectra all indicate changes in the cobalt coordination suggestive of a four-coordinate "base-off" conformation when cobalamin binds to an ATP:hATR complex (*28*, *29*). Because the DMB tail is inherently very flexible, there is a wide range of potential base-off conformations. The conformation of the DMB tail shown for our model is especially speculative and is only included in order to provide a sense of scale.

Our model of docked cobalamin is approximate but illustrates that the cleft formed upon ATP binding is an appropriate size and shape to accommodate the cobalamin ring and that invariant residues are suitably positioned to make important interactions (Figure 5). The only constraints on the docking are placing the cobalt atom ~3−4 Å away from the target carbon (C5*) of the ATP and avoidance of obvious steric clashes. In our model, the upper axial position of the cobalt points toward the ATP and the DMB tail, extending off ring D, points toward solvent. The plane of the macrocycle is positioned such that rings A and B are inserted into the cleft. In this conformation, the invariant phenylalanine residues below the active site are in a position to interact with the lower corrin ring structure and Phe170 in particular may assist with exclusion of solvent below the cobalt. No polar amino acid residue appears to be available to interact with the cobalt ion from the lower face as a replacement for the benzimidazole, consistent with the earlier conclusion that the DMB is not replaced by a protein residue (*28*, *29*).

Known Methylmalonic Aciduria Mutations. Mutations in hMMAB that contribute to disease have been identified in methylmalonic aciduria patients at positions Gly97*, Ser174, Arg186*, Arg190*, Arg191*, Glu193*, and Gln234 (* indicates invariant residues listed in Table 2) (*20*, *22*, *23*). Mutations in MMA patients have also been observed at Arg19 in the mitochondrial targeting sequence and at nonconserved positions Ala135, Ser180, and Tyr219. The functional significance of these mutations is unclear, however, because they have only been found in patients that are heterozygous for mutations in an invariant residue. Amino acid substitutions at Gly97 or Ser174, or a stop codon at position Gln234, would disrupt the orientation of the α3−α4 loop at the bottom of the active site. The most common mutation is a substitution of Arg186 for Trp or Gln. This arginine does not contact ATP in the structure but rather lies below the ATP in the cobalamin binding site and appears well positioned to interact with the cobalamin directly (Figures 3e,f and 5). As described above, Arg190 forms hydrogen bonds with the ATP and orients the C5* atom for catalysis. Arg191 is an invariant residue involved in the charged trimer interface. Mutation to Trp or Ala does not eliminate trimer formation but does knock out or reduce catalytic activity, while increasing the K_m for ATP 3-fold over wild-type levels (*20*, *22*, *25*). Clearly, the trimeric interface is crucial for adenosyltransferase activity. Finally, Glu193 is involved in coordinating the physiological Mg^{2+} ion, and mutation to Lys would inhibit ATP binding.

In summary, our structure of the hATR−ATP complex explains the importance of residues found mutated in methylmalonic aciduria patients and suggests a role for each of the invariant residues in stabilizing the structure, binding ATP, binding cobalamin, or in catalysis (Table 2). This advance will facilitate future studies aimed at understanding the mechanism of the ATR enzymes.

ACKNOWLEDGMENT

We thank Anne Heroux for data collection at the National Synchrotron Light Source Brookhaven National Laboratory, beamline x26c.

SUPPORTING INFORMATION AVAILABLE

Sequence alignment of PduO-like ATRs. This material is available free of charge via the Internet at http://pubs.acs.org.

REFERENCES

1. Banerjee, R., Ed. (1999) In *Chemistry and Biochemistry of B_{12}*, John Wiley and Sons, New York.
2. Roth, J. R., Lawrence, J. G., and Bobik, T. A. (1996) Cobalamin (coenzyme B_{12}): synthesis and biological significance, *Annu. Rev. Microbiol. 50*, 137−181.

3. Kräutler, B. (1997) B_{12} Coenzymes, the Central Theme, in *Vitamin B_{12} and B_{12}-Proteins* (Kräutler, B., Arigoni, D, and Golding, B.T., Eds.) pp 3−43, Wiley−VCH, New York.
4. Cauthen, S. E., Foster, M. A., and Woods, D. D. (1966) Methionine synthesis by extracts of *Salmonella typhimurium*, *Biochem. J. 98*, 630−635.
5. Drummond, J. T., and Matthews, R. G. (1993) Cobalamin-dependent and cobalamin-independent methionine synthases in *Escherichia coli*: two solutions to the same chemical problem, *Adv. Exp. Med. Biol. 338*, 687−692.
6. Banerjee, R., and Chowdhurry, S. (1999) Methylmalonyl-CoA Mutase, in *Chemistry and Biochemistry of B_{12}* (Banerjee, R., Ed.) pp 707−730, John Wiley and Sons, New York.
7. Pezacka, E. H. (1993) Identification and characterization of two enzymes involved in the intracellular metabolism of cobalamin. Cyanocobalamin beta-ligand transferase and microsomal cob(III)-alamin reductase, *Biochim. Biophys. Acta*. *1157*, 167−177.
8. Watanabe, F., Saido, H., Yamaji, R., Miyatake, K., Isegawa, Y., Ito, A., Yubisui, T., Rosenblatt, D. S., and Nakano, Y. (1996) Mitochondrial NADH- or NADPH-linked aquacobalamin reductase activity is low in human skin fibroblasts with defects in synthesis of cobalamin coenzymes, *J. Nutr. 126*, 2947−2951.
9. Seetharam, B. (1999) Receptor-mediated endocytosis of cobalamin (vitamin B_{12}), *Annu. Rev. Nutr. 19*, 173−195.
10. Banerjee, R. (2006) B_{12} Trafficking in Mammals: A Case for Coenzyme Escort Service, *ACS Chem. Biol. 1*, 149−159.
11. Rosenberg, L. E. (1983) in *The Metabolic Basis of Inherited Disease*, 5th ed., pp 474−497, McGraw-Hill, New York.
12. Rosenblatt, D. S., and Fenton, W. A. (2001) in *The Metabolic and Molecular Bases of Inherited Disease* (Scriver, C. R., Beaudet, A. L., Valle, D., and Sly, W. S., Eds.) pp 3897−3933, McGraw-Hill, New York.
13. Chandler, R. J., and Venditti, C. P. (2005) Genetic and genomic systems to study methylmalonic acidemia, *Mol. Genet. Metab. 86*, 34−43.
14. Kapadia, C. R. (1995) Vitamin B_{12} in Health and Disease; Part-1 Inherited Disorders of Function, Absorption and Transport, *The Gastroenterologist 3*, 329−344.
15. Shevell, M. I., and Rosenblatt, D. S. (1992) The neurology of cobalamin, *Can. J. Neurol. Sci. 19*, 472−486.
16. Watkins, D., and Rosenblatt, D. S. (2001) Cobalamin and Inborn Errors of Cobalamin Absorption and Metabolism, *The Endocrinologist 11*, 98−104.
17. Ledley, F. D., Lumetta, M., Nguyen, P. N., Kolhouse, J. F., and Allen, R. H. (1988) Molecular cloning of L-methylmalonyl-CoA mutase: gene transfer and analysis of *mut* cell lines, *Proc. Natl. Acad. Sci. U.S.A. 85*, 3518−3521.
18. Dobson, C. M., Wai, T., Leclerc, D., Wilson, A., Wu, X., Dore, C., Hudson, T., Rosenblatt, D. S., and Gravel, R. A. (2002) Identification of the gene responsible for the cblA complementation group of vitamin B_{12}-responsive methylmalonic acidemia based on analysis of prokaryotic gene arrangements, *Proc. Natl. Acad. Sci. U.S.A. 99*, 15554−15559.
19. Fenton, W. A., and Rosenberg, L. E. (1981) The defect in the *cblB* class of human methylmalonic acidemia: deficiency of cob(I)alamin adenosyltransferase activity in extracts of cultured fibroblasts, *Biochem. Biophys. Res. Commun. 98*, 283−289.
20. Dobson, C. M., Wai, T., Leclerc, D., Kadir, H., Narang, M., Lerner-Ellis, J. P., Hudson, T. J., Rosenblatt, D. S., and Gravel, R. A. (2002) Identification of the gene responsible for the *cblB* complementation group of vitamin B_{12}-dependent methylmalonic aciduria, *Hum. Mol. Genet. 11*, 3361−3369.
21. Leal, N. A., Park, S. D., Kima, P. E., and Bobik, T. A. (2003) Identification of the human and bovine ATP:Cob(I)alamin adenosyltransferase cDNAs based on complementation of a bacterial mutant, *J. Biol. Chem. 278*, 9227−9234.
22. Zhang, J., Dobson, C. M., Wu, X., Lerner-Ellis, J., Rosenblatt, D. S., and Gravel, R. A. (2006) Impact of cblB mutations on the function of ATP:cob(I)alamin adenosyltransferase in disorders of vitamin B_{12} metabolism, *Mol. Genet. Metab. 87*, 315−322.
23. Lerner-Ellis, J. P., Gradinger, A. B., Watkins, D., Tirone, J. C., Villeneuve, A., Dobson, C. M., Montpetit, A., Lepage, P., Gravel, R. A., and Rosenblatt, D. S. (2006) Mutation and biochemical analysis of patients belonging to the *cblB* complementation class of vitamin B_{12}-dependent methylmalonic aciduria, *Mol. Genet. Metab. 87*, 219−225.
24. Johnson, C. L., Pechonick, E., Park, S. D., Havemann, G. D., Leal, N. A., and Bobik, T. A. (2001) Functional genomic, biochemical, and genetic characterization of the *Salmonella* pduO gene, an ATP: cob(I)alamin adenosyltransferase gene, *J. Bacteriol. 183*, 1577−1584.
25. Saridakis, V., Yakunin, A., Xu, X., Anandakumar, P., Pennycooke, M., Gu, J., Cheung, F., Lew, J. M., Sanishvili, R., Joachimiak, A., Arrowsmith, C. H., Christendat, D., and Edwards, A. M. (2004) The Structural Basis for Methylmalonic Aciduria, *J. Biol. Chem. 279*, 23646−23653.
26. Leal, N. A., Olteanu, H., Banerjee, R., and Bobik, T. A. (2004) Human ATP:Cob(I)alamin adenosyltransferase and its interaction with methionine synthase reductase, *J. Biol. Chem. 279*, 47536−47542.
27. Fonseca, M. V., and Escalante-Semerena, J. C. (2001) An *in vitro* reducing system for the enzymic conversion of cobalamin to adenosylcobalamin, *J. Biol. Chem. 276*, 32101−32108.
28. Stich, T. A., Yamanishi, M., Banerjee, R., and Brunold, T. C. (2005) Spectroscopic Evidence for the Formation of a Four-Coordinate Co^{2+} Cobalamin Species upon Binding to the Human ATP:Cobalamin Adenosyltransferase, *J. Am. Chem. Soc. 127*, 7660−7661.
29. Yamanishi, M., Labunska, T., and Banerjee, R. (2005) Mirror "Base-Off" Conformation of Coenzyme B_{12} in Human Adenosyltransferase and its Downstream Target, Methylmalonyl-CoA Mutase, *J. Am. Chem. Soc. 127*, 526−527.
30. Lexa, D., and Seveant, J.-M. (1983) The electrochemistry of vitamin B_{12}, *Acc. Chem. Res. 16*, 235−243.
31. Stich, T. A., Buan, N. R., Escalante-Semerena, J. C., and Brunold, T. C. (2005) Spectroscopic and Computational Studies of the ATP: Corrinoid Adenosyltransferase (CobA) from *Salmonella enterica*: Insights into the Mechanism of Adenosylcobalamin Biosynthesis, *J. Am. Chem. Soc. 127*, 8710−8719.
32. Bauer, C. B., Fonseca, M. V., Holden, H. M., Thoden, J. B., Thompson, T. B., Escalante-Semerena, J. C., and Rayment, I. (2001) Three-Dimensional Structure of ATP:Corrinoid Adenosyltransferase from *Salmonella typhimurium* in its Free State, Complexed with MgATP, or Complexed with Hydroxycobalamin and MgATP, *Biochemistry 40*, 361−374.
33. Studier, F. W. (2005) Protein production by auto-induction in high density shaking cultures, *Protein Expr. Purif. 41*, 207−234.
34. McCoy, A., Grosse-Kunstleve, R., Storoni, L., and Read, R. (2005) Likelihood-enhanced fast translation functions, *Acta Crystallogr. D61*, 458−464.
35. Otwinowski, Z. (1993) Oscillation data reduction program, in *Data Collection and Processing* (Sawyer, L., Isaacs, N., and Bailey, S., Eds.) pp 56−62, SERC Daresbury Laboratory, Warrington, U.K.
36. CCP4. (1994) The CCP4 Suite: Programs for Protein Crystallography, *Acta Crystallogr. D50*, 760−763.
37. Jones, T. A., Zou, J. Y., Cowan, S. W., and Kjeldgaard, M. (1991) Improved methods for building protein models in electron density maps and the location of errors in these models, *Acta Crystallogr. A47*, 110−119.
38. Emsley, P., and Cowtan, K. (2004) Coot: model-building tools for molecular graphics, *Acta Crystallogr. D60*, 2126−2132.
39. Murshudov, G. N., Vagin, A. A., and Dodson, E. J. (1997) Refinement of Macromolecular Structures by the Maximum-Likelihood Method, *Acta Crystallogr. D53*, 240−255.
40. Holm, L., and Sander, C. (1998) Touring protein fold space with Dali/FSSP, *Nucl. Acids Res. 26*, 316−319.
41. Krissinel, E., and Henrick, K. (2004) Secondary-structure matching (SSM), a new tool for fast protein structure alignment in three dimensions, *Acta Crystallogr. D60*, 2256−2268.
42. Andreeva, A., Howorth, D., Brenner, S. E., Hubbard, T. J. P., Chothia, C., and Murzin, A. G. (2004) SCOP database in 2004: refinements integrate structure and sequence family data, *Nucl. Acids Res. 32*, D226−D229.
43. Sanishvili, R., Pennycooke, M., Gu, J., Xu, X., Joachimiak, A., Edwards, A. M., and Christendat, D. (2004) Crystal structure of the hypothetical protein TA1238 from *Thermoplasma acidophilum*: A new type of helical super-bundle, *J. Struct. Funct. Genomics 5*, 231.
44. Suh, S., and Escalante-Semerena, J. C. (1995) Purification and initial characterization of the ATP:corrinoid adenosyltransferase encoded by the cobA gene of *Salmonella typhimurium*, *J. Bacteriol. 177*, 921−925.
45. DeLano, W. L. (2002) DeLano Scientific, San Carlos, CA, U.S.A.

BI061396F

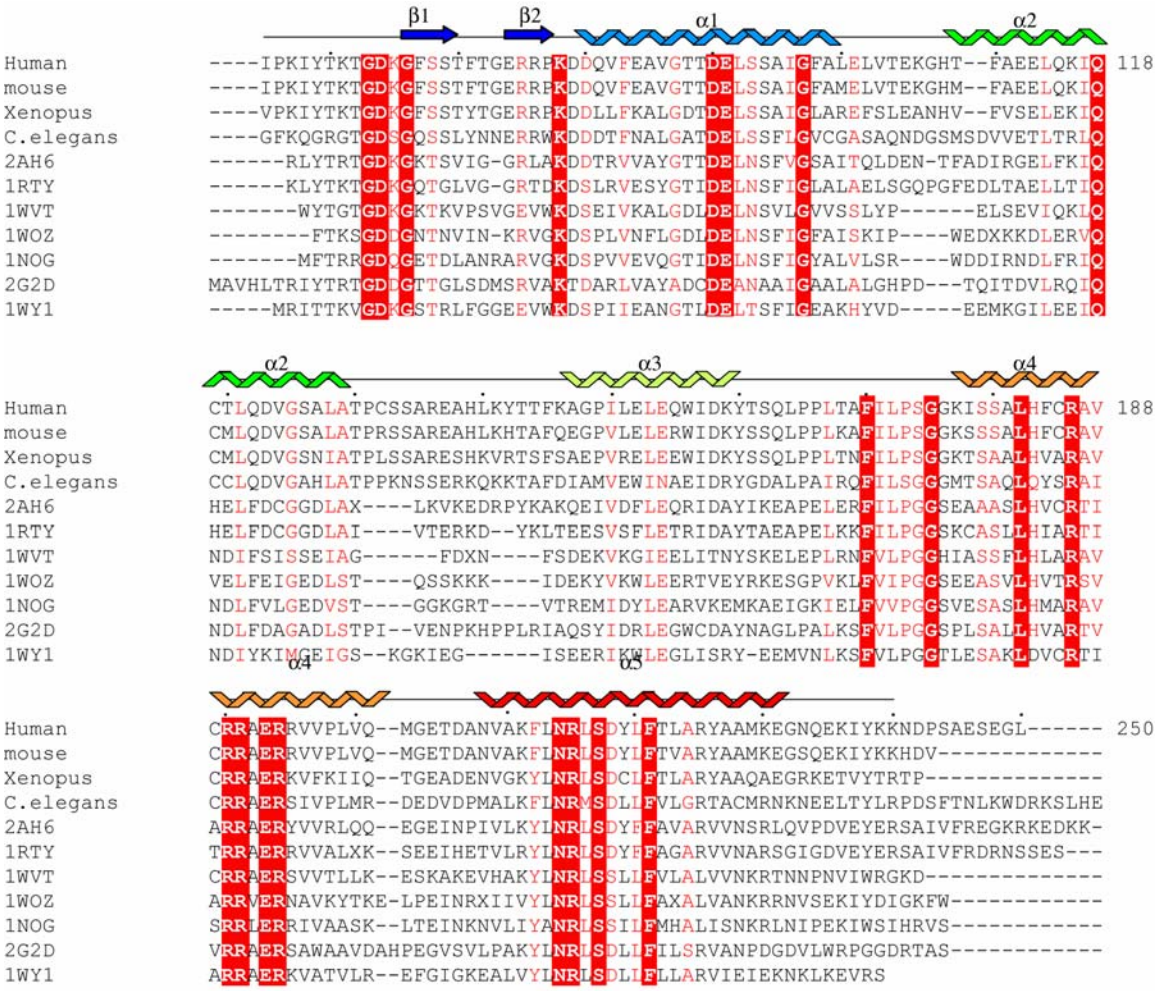

Supplemental Data

Figure 1.

Sequence alignment of PduO-like ATRs. Secondary structure and numbering of hATR is indicated above the alignment, and conserved residues (red on white) and invariant residues (white on red) are highlighted. Sequences are from human (AAH05054.1), mouse (BAE28544.1), xenopus (AAI06514.1), *C.elegans* (AAA21165.2), *Bacillus Halodurans* (10174212) PDBcode:2AH6, *Bacillus Subtilis* Yvqk PDBcode:1RTY, *Sulfolobus Tokodaii* (St2180) PDBcode:1WVT, *Sulfolobus Tokodaii* St1454 PDBcode:1WOZ, *Thermoplasma Acidphilum* TA0546 PDBcode 1NOG, *Mycobacterium Tuberculosis* PDBcode:2GDG. *Pyrococcus horikoshi* OT3 PH0671 PDBcode:1WY1.